RSC Advances

ROYAL SOCIETY OF CHEMISTRY

www.rsc.org/advances

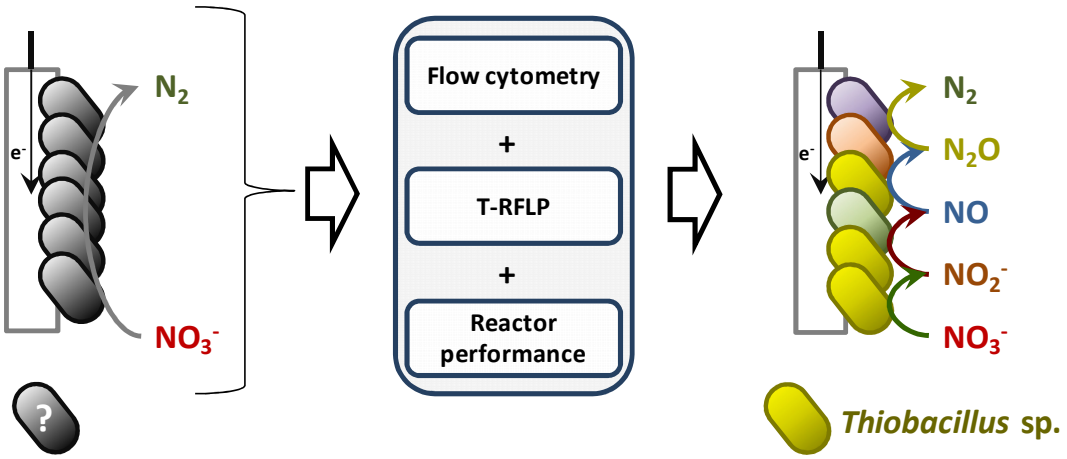

Elucidating the structure-function relationship of a denitrifying biocathode

Journal Name

ARTICLE

Monitoring and engineering reactor microbiomes of denitrifying bioelectrochemical systems†

Received 00th January 20xx,
Accepted 00th January 20xx

DOI: 10.1039/x0xx00000x

www.rsc.org/

N. Pous,[a] C. Koch,[b] A. Vilà-Rovira,[a] M.D. Balaguer,[a] J. Colprim,[a] J. Mühlenberg,[c] S. Müller,[b] F. Harnisch[b] and S. Puig[*,a]

Denitrifying bioelectrochemical systems (d-BES) are a promising technology for nitrate removal from wastewaters. Microbial community monitoring is required to pave the way to application. In this study, for the first time flow cytometry combined with molecular biology techniques is exploited to monitor and determine the structure-function relationship of the microbiome of a denitrifying biocathode. Stable cathode performance at poised potential (-0.32 V vs Ag/AgCl) was monitored, and different stress-tests were applied (reactor leakage, nitrate concentration, buffer capacity). Stress-tests shifted the reactor microbiome and performance. The monitoring campaign covered a wide range of nitrate consumption rates (from 15 to 157 $mgN \cdot L^{-1}_{NCC} \cdot d^{-1}$), current densities (from 0 to 25 $mA \cdot L^{-1}_{NCC}$) and denitrification intermediates (nitrite and nitrous oxide consumption rates varied from 0 to 56 $mgN \cdot L^{-1}_{NCC} \cdot d^{-1}$). The reactor microbiome (composed of 21 subcommunities) was characterized and its structure-function relationship was revealed. A key role for *Thiobacillus* sp. in the bioelectrochemical reduction of nitrate is suggested, while a wider number of subcommunities were involved in NO_2^- and N_2O reduction. It was demonstrated that different bacteria catalyze each denitrification step in a biocathode. This study contributed significantly on understanding denitrifying biocathodes, paving the way for its knowledge-driven engineering.

Introduction

Nitrate (NO_3^-) is an abundant and harmful inorganic contaminant, which is present in waste water, surface water and groundwater.[1,2] Microbial electrochemical technologies (METs) are an innovative and promising technology platform which reactors are usually termed bioelectrochemical systems (BES).[3] METs allow, among other applications, the removal of inorganic contaminants,[4,5] like hexavalent uranium, arsenite or hexavalent chromium.[6-8] For BES-based nitrate removal, biological autotrophic denitrification is performed in a biocathode, where bacteria reduce nitrate using the cathode as electron donor.[9] Nitrate is reduced to dinitrogen gas (N_2) in a four-step reduction reaction, where nitrite (NO_2^-) and nitrous oxide (N_2O) are stable, environmentally even more harmful, intermediates.

Denitrifying-BES (d-BES) have evolved during the last years from the proof of concept to application in technological oriented research aiming for higher denitrification rates. The knowledge about d-BES engineering includes different reactor designs,[10,11] the effect of some key parameters (such as pH or conductivity),[12,13] or different bioelectrochemical configurations (autonomous microbial fuel cell mode,[10,11] or energy demanding microbial electrolysis mode)[14,15]. However, knowledge regarding the microbiome role (i.e. which subcommunitites perform each nitrate reduction step) on bioelectrochemical denitrification is scarce.

Molecular analyses have shown so far that diverse communities are found in denitrifying biocathodes.[14,16-18] Like for anodes,[19] an electrochemically driven selection takes place at denitrifying microbial cathodes, leading usually to the enrichment of different species of Proteobacteria.[16-18] However, which microorganisms catalyze which reduction reaction in the denitrifying process has not been elucidated, yet. Abundances variation of responsible subcommunities may clarify the successive reductive processes in d-BES. Therefore, it is essential to study the reactor performance together with the subcommunities` dynamics (i.e. cell abundances). A whole arsenal of techniques for investigating electroactive microbial biofilms is available.[20] Whereby the combination of techniques for phylogenetic analysis (16S rDNA terminal restriction fragment length polymorphisms (T-RFLP) analysis and sequencing) and cytometric DNA/scatter-plot distributions using flow cytometry have been demonstrated to allow monitoring and deriving structure-function relationships of reactor microbiomes.[21] The use of flow cytometry is based on DNA staining for fluorescence detection, allowing the analysis of every single cell present in the sample.[22] Each cell is detected, classified in microbial subcommunities (marked as gates) and, finally, quantified within the subcommunities.

In this article, we aimed to use cytometric fingerprinting combined with 16S rDNA analysis to monitor community

[a] LEQUiA, Institute of the Environment, University of Girona, Campus Montilivi, E-17071 Girona, Catalonia, Spain. E-mail: sebastia@lequia.udg.cat; Tel:+34972418281
[b] Helmholtz Centre for Environmental Research – UFZ, Department of Environmental Microbiology, Permoserstraße 15 I 04318 Leipzig, Germany
[c] DBFZ Deutsches Biomasseforschungszentrum gemeinnützige GmbH, Torgauer Straße 116, 04347 Leipzig, Germany

† Electronic Supplementary Information (ESI) available: [details of any supplementary information available should be included here]. See DOI: 10.1039/x0xx00000x

dynamics during denitrification at a biocathode. A d-BES was constructed, operated and monitored. Shifts on bacterial activity were provoked by the application of different stress-tests simulating events that are likely to occur in a full-scale application: a reactor leakage (loss of suspended biomass), a power shutdown (break down of bioelectrochemical nitrate reduction) and alteration of influent qualities (pH, conductivity, nitrate concentration, hydraulic retention time). Data obtained from the microbiome was evaluated together with computational fluid dynamics and reactor performance (nitrogen consumption rates, current density, coulombic efficiency) and used to reveal the microbial structure-function relationship of the denitrifying biocathode.

Experimental

Experimental set-up

A two-chamber d-BES, similar to Pous et al.,[23] was built using two methacrylate frames (200 mm x 200 mm x 22 mm) separated by cation exchange membrane (20 x 20 cm, CMI-7000, Membranes Int., USA). The cathode contained granular graphite (diameter 1.5 - 5 mm, EnViro-cell, Germany) and one graphite rod (250 mm x 6 mm, Mersen Ibérica, Spain). The anode contained one stainless steel rod (250 mm x 6 mm) and stainless steel mesh (20 x 20 cm, path 5 x 5 mm, Mersen Ibérica, Spain). Net anodic compartment (NAC) and net cathodic compoartment (NCC) volumes were 784 mL and 420 mL, respectively. The cathode compartment contained an Ag/AgCl reference electrode (+0.197 V vs standard hydrogen electrode (SHE), model RE-5B BASi, USA). Influents were continuously fed at 566±9 $mL \cdot d^{-1}$. An internal recirculation loop (94±4 $L \cdot d^{-1}$) was placed in each compartment (Figure 1A). Anodic and cathodic hydraulic retention times (HRT) were 1.3 and 0.7 days, respectively. Experiments were performed at room temperature (22ºC).

The cathode was fed with synthetic medium prepared with deionized water. It contained 1.21 $g \cdot L^{-1}$ $NaNO_3$ (equivalent nitrogen concentration of 200 $mgN\text{-}NO_3^- \cdot L^{-1}$); 1.00 $g \cdot L^{-1}$ $NaHCO_3$ as inorganic carbon source; 1.55 $g \cdot L^{-1}$ $Na_2HPO_4 \cdot 7H_2O$ and 0.58 $g \cdot L^{-1}$ $KH_2PO_4 \cdot H_2O$ (10 mM phosphate buffer solution (PBS)); 0.50 $g \cdot L^{-1}$ NaCl; 0.10 $g \cdot L^{-1}$ $MgSO_4 \cdot 7H_2O$; 0.02 $g \cdot L^{-1}$ $CaCl_2$; 0.02 $g \cdot L^{-1}$ NH_4Cl; 0.1 $mL \cdot L^{-1}$ trace nutrients.[24] The anode was fed with the same medium without $NaNO_3$. Anodic and cathodic specific conductivities were 5.3±0.1 and 4.0±0.1 $mS \cdot cm^{-1}$, respectively. Media was sparged with N_2 during 15 minutes prior feeding.

The cathode potential (i.e. working electrode) was poised at -0.32 V vs Ag/AgCl (-0.12 V vs. SHE) by a potentiostat (models SP-50 and VMP3, Bio-logic, France) based on previous studies.[25] Current was normalized to NCC and expressed as current density (*j*). The current flow was negative (cathodic process); for improved graphical representation as well as correlation analysis absolute current densities were used ($|j|$).

Inoculation and operation

For the cathode's inoculation, the cathode was connected in a closed-loop mode to a tank containing 2500 mL of cathode medium and 125 mL of activated sludge (Girona's WWTP, Spain). The tank's medium was replaced with fresh cathode medium when nitrate was consumed. After three medium replacements, the inoculation procedure finished (41 days), and the cathode was fed at continuous-flow mode during 15 days (in Girona) to allow complete stabilization of the microbial community. Then, the d-BES was sent to Leipzig. During the travel (4 days), the d-BES was under open circuit conditions. Then, the d-BES was operated at continuous-flow mode as well and different stress-tests (details below and in

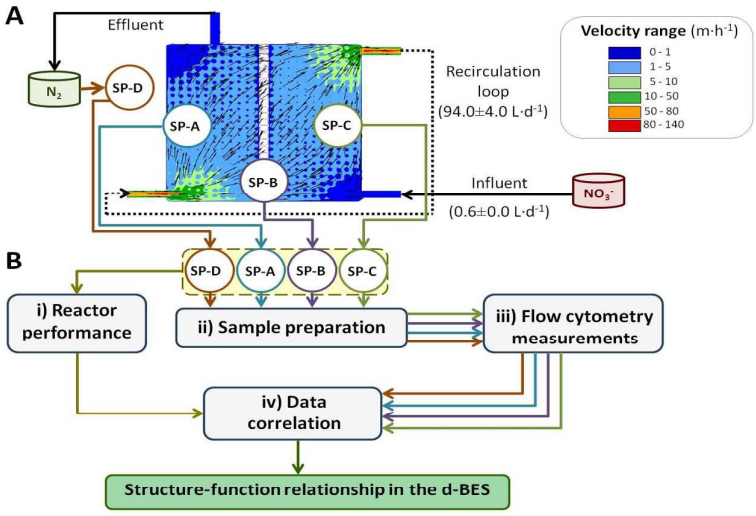

Figure 1. A) Representation of the cathode compartment showing influent/effluent and recirculation flows, the fluid dynamics (velocity and direction inside the cathode) and the positions of sampling ports (SP). B) Flow diagram for determining the structure-function relationship in the d-BES: i) Reactor performance was determined in terms of ΔNO_3^-, ΔNO_2^-, ΔN_2O, current density and *CE*; ii) Samples for microbial analysis were fixated, washed and stained with DAPI; iii) Stained samples were analysed by flow cytometry and resulting data interpreted by gating and calculating the cell abundances of each gate; iv) Cytometric and reactor performance data were correlated to elucidate the structure-function relationship of the cathode.

Figure 2A) were applied to stimulate dynamics on denitrifying activity. Samples were taken every three days. At every new stress-test, the system was operated at least three times the hydraulic retention time before taking the first sample (steady-state conditions).

Different scenarios that could arise during operation of the BES, denominated as stress-test- and abbreviated as ST-, were applied:

ST-0)Reactor leakage (days 26 to 29): The cathode volume was withdrawn, removing the suspended biomass and exposing the cathode to oxygen. The purpose was to evaluate the contribution of suspended biomass and the impact of oxygen on the denitrifying microbiome and the d-BES performance.

ST-1) Activity reawakening (days 29 to 38): In this test, the recovery of activity after the reactor leakage was followed.

ST-2)Activity stabilization (days 39 to 55): System recovery after the reactor leakage until reaching stable activity (stable current density and nitrate consumption rate) was assured before applying further stress-tests.

ST-3)Influence of influent pH (days 55 to 61): The influent pH was modified from 7.6 to 7.1 to assess its influence on the denitrifying activity.

ST-4) Impact of buffer capacity/ conductivity (days 61 to 63, 67 to 90 and 95 to 97): The media composition was changed by increasing the PBS concentration from 10 mM to 20 mM in order to check both buffer and conductivity influence on bioelectrochemical denitrification.

ST-5)Power shutdown (days 63 to 67): Operation at open circuit potential (OCP) to distinguish between bioelectrochemical and non-bioelectrochemical activities.

ST-6)Impact of hydraulic retention time (days 90 to 95): The influent flow rate was lowered from 566±0 to 283±0 mL·d^{-1}. Thus, the nitrate loading rate (NO_3^-LR) was decreased from 279±5 to 140±0 mgN-NO_3^-·L^{-1}·d^{-1}. This test evaluated the influence of increasing the hydraulic retention time in bioelectrochemical denitrification.

ST-7)Influence of influent nitrate concentration (days 97 to 104): The nitrate concentration was lowered from 205±4 to 104±2 mgN-NO_3^-·L^{-1}. Accordingly, the NO_3^-LR was decreased from 279±5 to 141±2 mgN-NO_3^-·L^{-1}·d^{-1}. The purpose of this test was to evaluate the impact of nitrate availability at constant HRT on the denitrifying process.

The anode was not inoculated and always fed at continuous-flow mode. Abiotic oxidations, e.g. oxygen evolution from water electrolysis, occurred at the anode.[25]

Analytical methods and calculations

Nitrate and nitrite concentrations were analyzed using photometric tests (114563-NO_3^- spectroquant®, 100609-NO_2^- spectroquant®; Merck, Germany). In Girona, the N_2O content was analyzed with a nitrous oxide microsensor (Unisense, Denmark) located at the cathode recirculation loop. In Leipzig, the N_2O content was analyzed using a gas chromatograph with headspace autosampler and electron capture detector (Agilent Technologies, USA) as explained in supplementary information S1. The influent nitrate loading rate (NO_3^-LR) was calculated by dividing the influent nitrate concentration per HRT.

The nitrate, nitrite and nitrous oxide consumption rates (ΔNO_3^-, ΔNO_2^- and ΔN_2O, respectively) were calculated as shown in eqn (1 - 3). Nitric oxide accumulation was considered negligible.[15]

$$\Delta NO_3^- = \frac{CNO_3^-{}_{influent} - CNO_3^-{}_{effluent}}{HRT}; (1)$$

$$\Delta NO_2^- = \Delta NO_3^- - \frac{CNO_2^-{}_{effluent}}{HRT}; (2)$$

$$\Delta N_2O = \Delta NO_2^- - \frac{CN_2O_{effluent}}{HRT}; (3)$$

where $CNO_3^-{}_{influent}$, $CNO_3^-{}_{effluent}$, $CNO_2^-{}_{effluent}$ and $CN_2O_{effluent}$ accounts for nitrate, nitrite and nitrous oxide concentrations at influent or effluent (either mgN·L^{-1} or mmolN·L^{-1}).

The coulombic efficiency (*CE*) calculation (eqn. 4) was adapted from Virdis et al.[15] considering the required number of electrons for each sequential step from NO_3^- to N_2: nitrate to nitrite (NO_3^-/NO_2^-), nitrite to nitrous oxide (NO_2^-/N_2O) and nitrous oxide to dinitrogen gas (N_2O/N_2).

$$CE = \frac{t \cdot i}{NCC \cdot F \cdot \left(n_{NO_3^-/NO_2^-} \cdot \Delta NO_3^- + n_{NO_2^-/N_2O} \cdot \Delta NO_2^- + n_{N_2O/N_2} \cdot \Delta N_2O\right)}; (4)$$

where *i* is absolute current (mA); *t* is the time-converting factor between seconds and hours (3600); *NCC* is the cathode liquid volume (L); *F* is the Faraday's constant (96485 C•mol-e$^-$ ^{1}); *n* is the number of electrons required for each reaction (nNO_3^-/NO_2^- = 2, nNO_2^-/N_2O = 2 and nN_2O/N_2 = 1); ΔNO_3^-, ΔNO_2^- and ΔN_2O are the consumption rates expressed in mmolN·L^{-1}$_{NCC}$·h^{-1}.

A

Stress-test	1	2	3	4	5	6	7
Influent pH	7.7±0.0	7.6±0.1	7.1±0.0	6.9±0.1	6.8±0.0	6.8±0.0	6.9±0.1
Influent PBS (mM)	10	10	10	20	20	20	20
Closed circuit?	Yes	Yes	Yes	Yes	No	Yes	Yes
HRT (days)	0.7±0.0	0.7±0.0	0.7±0.0	0.7±0.0	0.7±0.0	1.5±0.0	0.7±0.0
Influent [NO_3^-] (mgN-NO_3^-·L^{-1})	196±14	199±7	193±2	205±4	202±0	205±0	104±2
NO_3^-LR (mgN-NO_3^-·L^{-1}·d^{-1})	267±19	270±9	263±3	279±5	276±0	140±0	141±2

B

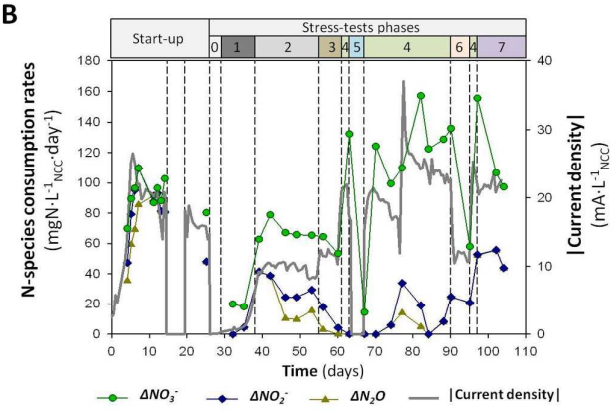

Figure 2. A) Conditions applied for each stress-test phase. B) Absolute current density and nitrate, nitrite and nitrous oxide consumption rates (ΔNO_3^-, ΔNO_2^- and ΔN_2O, respectively) during the continuous-flow mode operation.

Fluid hydrodynamics and microbiological sampling

The flows inside the cathode (Figure 1A) were calculated using computational fluid dynamics (Ansys Fluent v12.1)[26] as explained in supplementary information S2. The influent flow and the recirculation loop generated heterogeneous flows, suggesting zones with different nutrients availability (Figure 1A). Accordingly, samples for microbiological analyses were taken from three sampling ports of the cathode volume (denominated as SP-A, SP-B and SP-C), and from the cathode effluent (SP-D) as shown in Figure 1. The samples were taken using a needle to scratch the graphite granules surface (electrode), drawing a total volume of 6 mL for SP-B and SP-C, and 7 mL for SP-A (lower biomass observed).

Flow cytometry: measurements and data analyses

Cytometric measurements. The microbiome response to the different stress-tests was monitored. We combined cytometric DNA/scatter-plot distribution using flow cytometry and phylogenetic analysis (16S rDNA T-RFLP analysis and sequencing).[21]

Directly after sampling, the cells were fixated with a 2% paraformaldehyde solution and stained with DAPI according to Koch et al.[27] Cytometric measurements were performed as described in Koch et al.[21] All subcommunities of stained cells were marked with gates using a gate template (supplementary information S3) and their abundance changes followed over time.

Gate G2 of SP-C sample (day 95) was cytometrically sorted (200.000 cells) and further phylogenetically analysed.[21]

Cytometric data analyses. Cytometric data were statistically analyzed to elucidate the structure-function relationship of the cathode microbiome.[21,28]

To reveal electroactive subcommunities, the cell abundance of each gate was normalized to its cell abundance in open circuit conditions (ST-5) (non-bioelectrochemical control). For a better visualization of higher and lower cell abundances, a log10 transformation was applied. In this way, cell abundance increases and decreases have the same distance to the value under open circuit conditions (0, color code grey in Figure 3). A tenfold higher cell number would be represented by 1 (dark green) and a tenfold lower cell number by -1 (dark red), respectively.

The functional relationship between cell abundances and reactor performance was investigated by generating correlation analyses. Correlations between the raw cell abundances and reactor performance (ΔNO_3^-, ΔNO_2^- and ΔN_2O, current density, *CE* and effluent pH) were calculated using a subset of data covering ST-4 and ST-5 (supplementary information S7) and the whole dataset (supplementary information S8).[21]

Molecular analyses. The samples were centrifuged (14.000 g) and the pellet was stored at -20 °C. DNA extraction, PCR amplification of 16S rDNA, T-RFLP analysis, cloning and sequencing were performed according to Koch et al.[27] PCR amplification of functional denitrification genes (napA, narG, nirK, nirS, nosZ) was done according to Vilar-Sanz et al.[17]

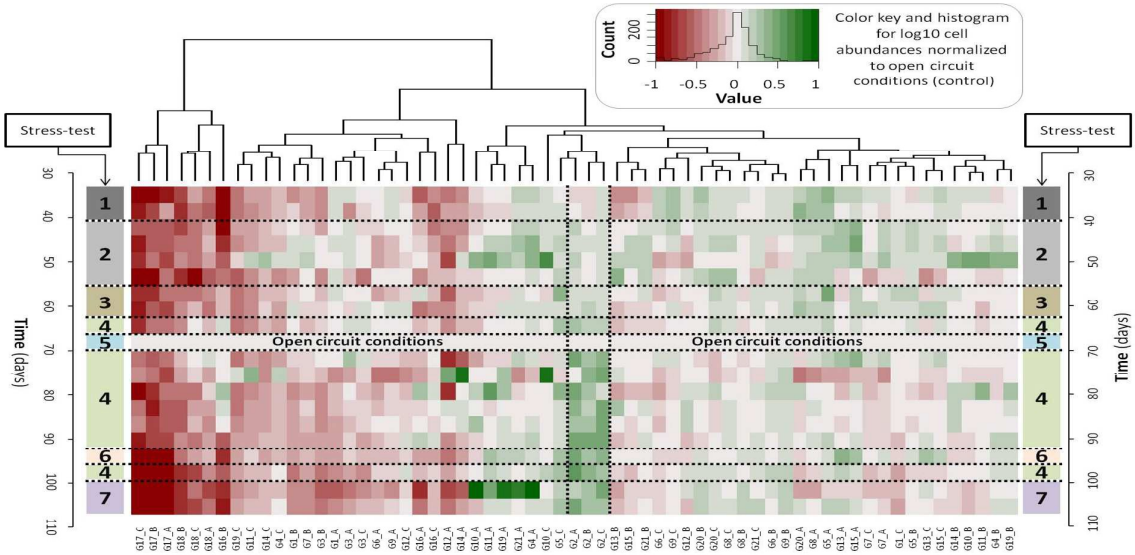

Figure 3. Microbiome dynamics during the different stress-test phases (from ST-1 to ST-7). The CyBar visualizes the cell abundance of individual subcommunities. Gates are labeled as G*X*_*Y*, where: *X* = gate number, and *Y* = sampling port. For a better visualization of higher and lower cell abundances, a log10 transformation was applied. Cell abundance increases and decreases have the same distance to the value under open circuit conditions (0, color code grey). A tenfold higher cell number is represented by 1 (color code dark green) and a tenfold lower cell number by -1 (color code dark red), respectively.

Results and discussion

BES start-up

The d-BES was operated under continuous-flow mode after the inoculation finished (Figure 2B, mean values and standard deviations in supplementary information S4). The absolute current density and nitrogen consumption rates (ΔNO_3^-, ΔNO_2^-, ΔN_2O) rapidly increased. The current density stabilized after 7 days at 21.7±1.4 mA·L-1$_{NCC}$, while ΔNO_3^- was 97.7±11.5 mgN·L$^{-1}_{NCC}$·d^{-1}. Nitrite and nitrous oxide reductions were also promoted, ΔNO_2^- and ΔN_2O were 96.9±11.4 and 90.1±4.0 mgN·L$^{-1}_{NCC}$·d^{-1}, respectively. A coulombic efficiency (*CE*) of 70.7±8.1% was observed.

When re-set to a potential of -0.32 V vs Ag/AgCl (see experimental, Figure 2B days 19-26) the electroactivity of the cathode decreased in terms of current density (from 21.7±1.4 mA·L$^{-1}_{NCC}$ (days 7-15) to now 14.9±1.4 mA·L$^{-1}_{NCC}$). Interestingly, different affections on denitrification were observed. The ΔNO_2- decreased significantly by 33.5% (from 90.1±4.0 to 64.4±0.0 mgN·L$^{-1}_{NCC}$·d^{-1}), while ΔNO_3^- decreased only by 6.4% (from 97.7±11.5 to 91.5±0.0 mgN·L$^{-1}_{NCC}$·d^{-1}). Therefore, a denitrifying biocathode able to reduce NO_3^- to N_2 was obtained.

Reactor performance during different stress-tests

The influence of different stress types on the system performance was tested when the current density was stable for 7 days (days 19-26). Figure 2B shows the reactor performance evolution. Mean values and standard deviations for each stress-test are reported in supplementary information S4.

The reactor leakage (ST-0) led to system break-down and clearly affected the biocathode activity after re-feeding (ST-1). If activity at ST-1 is compared to the activity before the reactor leakage (start-up), it can be observed a decrease of the absolute current density (from 14.9±1.4 to 0.8±0.2 mA·L$^{-1}_{NCC}$) and ΔNO_3^- (from 91.5±0.0 to 19.0±1.3 mgN·L$^{-1}_{NCC}$·d^{-1}). Denitrification intermediates were also affected, ΔNO_2^- and ΔN_2O decreased from 64.4±0.0 to 2.3±3.2 mgN·L$^{-1}_{NCC}$·d^{-1} and from 64.4±0.0 to 2.3±3.2 mgN·L$^{-1}_{NCC}$·d^{-1}, respectively. Remarkably, the biocathode activity recovered quickly, without reintroducing the extracted cathode's bulk liquid or reinoculation, reaching stable current density at day 39 (ST-2 in Figure 2B) ($|j|$= 9.5±1.4 mA·L$^{-1}_{NCC}$), with a ΔNO_3^- of 68.0±6.2 mgN·L$^{-1}_{NCC}$·d^{-1}. These values were 36% and 26% lower than those observed before the reactor leakage. Besides nitrate reducing activity recovered, ΔNO_2^- and ΔN_2O did not (31.7±8.0 and 23.2±3.2 mgN·L$^{-1}_{NCC}$·d^{-1}, respectively), leading to NO_2^- and N_2O accumulation.

On day 55, media composition was changed to investigate the influence of pH stress (ST-3) and changing buffer capacity (ST-4). During stress-test 3, the pH of the influent decreased from 7.6 to 7.1 (ST-3), and negligible differences were observed in terms of current density and denitrifying activity (Figure 2B). The decrease on influent pH was too small, and the effluent pH remained stable at high values (9.1±0.4 in ST-2 and 9.2±0.2 in ST-3), very likely limiting the reactor performance.

Increase in buffer capacity (ST-4) from 10 to 20 mM PBS, increased the biocathodic activity as expected.[13] The absolute current density (22.8±2.0 mA·L$^{-1}_{NCC}$) and ΔNO_3^- (131.9±18.6 mgN·L$^{-1}_{NCC}$·d^{-1}) were almost doubled in comparison to ST-3. Besides promoting nitrate reduction, ΔNO_2^- remained almost stable (13.9±18.2 mgN·L$^{-1}_{NCC}$·d^{-1}), while ΔN_2O increased (from 1.5±2.1 to 12.0±18.2 mgN·L$^{-1}_{NCC}$·d^{-1}).

The simulation of a power shutdown (open circuit, ST-5) confirmed that the denitrifying activity was clearly related to electrochemical activity and thus linked to microbial electrocatalysis, as shown previously.[29] A low residual nitrate reduction was detected (ΔNO_3^- of 14.5 mgN·L$^{-1}_{NCC}$·d^{-1}; 1% of the maximum rate achieved), possibly related to endogenous heterotrophic denitrification.[30]

The influence of nitrate acting as electron acceptor was assessed by decreasing the nitrate loading rate (NO_3^-LR) from 279 to 140 mgN·L$^{-1}_{NCC}$·d^{-1} (ST-6 and ST-7). Two scenarios were tested: a decrease of the influent flow rate (ST-6) and a decrease of the influent nitrate concentration (ST-7).

When the influent flow rate was decreased, the absolute current density declined by 54% (from 22.8±2.0 to 10.6±0.0 mA·L$^{-1}_{NCC}$), and the ΔNO_3^- by 56% (from 131.9±18.6 to 58.0±0.0 mgN·L$^{-1}_{NCC}$·d^{-1}). On the contrary, when the influent nitrate concentration was lowered, the absolute current density and the ΔNO_3^- increased (23.1±0.7 mA·L$^{-1}_{NCC}$ and 102.0±6.6 mgN·L$^{-1}_{NCC}$·d^{-1}). The ΔNO_2^- was doubled (from 20.9±0.0 to 49.8±8.4 mgN·L$^{-1}_{NCC}$·d^{-1}) and no accumulation of N_2O was detected. Therefore, at the same NO_3^-LR, high HRTs decreased denitrification rates in comparison to low influent nitrate concentration, which supported denitrification rates. From the engineering perspective, it can be hypothesized that higher denitrification performances can be achieved by operating the system at lower HRTs.

The stress-tests caused variations on reactor performance. A wide range of ΔNO_3^-, ΔNO_2^-, ΔN_2O and current densities were detected in the same d-BES. Consequently, microbiome activity dynamics were expected as well.

Chemical-physical heterogeneity within the cathode volume

The application of computational fluid dynamics inside the cathode compartment showed flow heterogeneity (Figure 1A) and consequently, different N-species distribution (NO_3^-, NO_2^- and N_2O). The cathode's chemical-physical heterogeneity was investigated by analyzing the NO_3^- concentration and pH at each cathode volume sampling port (SP-A, -B and -C). The results obtained at each port were normalized to the value measured at the effluent (SP-D).

SP-C presented the highest relative availability of nitrate (1.05±0.01), while SP-A had the lowest (0.98±0.02). The pH was more homogeneous. The lowest relative pH ratio was at SP-C (0.99±0.00), while at SP-A and SP-B the same ratio (1.01±0.00) was presented. Thus, chemical-physical heterogeneity was observed, being SP-C the most favorable zone for nitrate reducing bacteria to grow.

Monitoring biocathode microbiome using flow cytometry

The stress-tests provoked dynamics on reactor performance (Figure 2B). Consequently, microbiome dynamics were also expected, and monitoring using flow cytometry and phylogenetic analysis was performed.[21]

For cytometric analysis a gate template was constructed consisting of 21 subcommunities (supplementary information S3). The cell abundances of each gate during the whole study can be found in supplementary information S5 (dataset) and S6 (box plot). Three subcommunities were predominant in all sampling ports (gates 2, 6 and 9 (G2, G6 and G9); with mean values of 18, 13 and 15%, respectively). Additionally, G1 was also abundant in SP-D (11%). In the following sections the cytometric data was used to elucidate the structure-function relationship in this d-BES.

Dynamics of cell abundances. The cell abundance dynamics are shown in Figure 3 and the evolution of cytometric measurements can be visualized in video 1. From a first sight it can be clearly seen that cell abundances of subcommunities changed in response to the different stress-tests (ST-1 to ST-7) as did the performance parameters (Figure 2B).

Some subcommunities presented higher cell abundance (shades of green) when the electrical circuit was closed (all phases except ST-5), while some did not (shades of red). Hence, in closed circuit conditions, some subcommunities benefited from the applied potential, and their cell abundance increased (e.g. G2_B, G5_C), while other subcommunities increased their relative cell abundance under open circuit conditions (ST-5) (e.g. G17_C, G18_B, G19_C). It suggests that only a portion of the microbial community was directly involved in the bioelectrochemical process.

Especially the cell abundance in G2 (G2 of all sampling ports evolved similar and grouped closely together) follows the course of ΔNO_3^- and current density over the different stress-test phases. During the recovery phase (ST-1) the cell abundance is comparable to ST-5 (power shutdown) while it increases over the other stress phases with highest abundances in ST-4 (cell abundance of G2 in all SPs of 21.1±6.0). As the dynamics of the highly abundant subcommunity G2 seem to follow the performance regarding nitrate reduction and current density, a relevant role of G2 for the bioelectrochemical nitrate reduction is indicated.

Correlating cell abundance with reactor performance. For a deeper understanding of subcommunities` dynamics, the correlation between the cell abundances and reactor performance was investigated.[27] To avoid overlapping effects of the different stress-tests, the specific case of recovery after a power shutdown is considered first. This case covers phases ST-4 and ST-5 (days 61 to 90) and, therewith, also the development during the longest stress with more data points enabling meaningful statistical analysis. Figure 4 visualizes the correlation of the three most abundant gates (G2, G6 and G9 of all sampling ports) with the reactor performance including nine time points. The results of all gates and respective

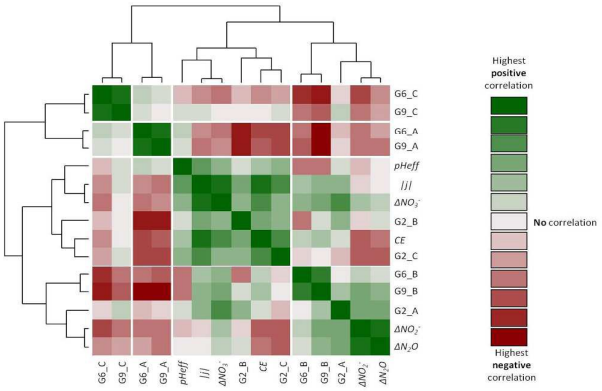

Figure 4. Correlation of the most abundant subcommunities G2, G6 and G9 with reactor performance using Spearman's rank correlation in ST-4 and ST-5 phases. Strong positive correlation is indicated by color code dark green. Strong negative correlation is indicated by color code dark red. The different gates have been labeled as G*X*_*Y*, where: *X* = gate number and *Y* = sampling port. Reactor performance included: pH at cathode effluent (*pHeff*), absolute current density (*|j|*), coulombic efficiency (*CE*) and nitrate, nitrite and nitrous oxide consumption rates (ΔNO_3^-, ΔNO_2^- and ΔN_2O, respectively).

correlation values can be found in supplementary information S7. The following gate correlations for this case are discussed: i) nitrate consumption rate (ΔNO_3^-); ii) reduction of denitrification intermediates (ΔNO_2^- and ΔN_2O); and iii) absolute current density and *CE*. Correlations higher than moderate positives correlations were considered (> 0.4).[31]

Correlation analyses (Figure 4 and supplementary information S7) shows a moderate to high correlation of subcommunity G2 to ΔNO_3^- for all sampling ports (0.5 – 0.7). Other subcommunities also presented at least moderate correlation to ΔNO_3^- (G6_B, G9_B, G5_C, G8_C and G21_C), but this behaviour was not homogeneous in all sampling ports (e.g. G6_A and G9_A showed no correlation to ΔNO_3^- (-0.1)).

For complete denitrification, NO_2^- and N_2O reduction have to be considered, as these are environmentally harmful. ΔNO_2^- and ΔN_2O increased in ST-4 in comparison to the power shutdown (ST-5), but the consumption rates were in range of the other stress-test. None of the gates showed positive correlations in all sampling ports for ΔNO_2^- or ΔN_2O suggesting heterogeneities of NO_2^- and N_2O concentration in the d-BES, which is in accordance with the flow heterogeneity discussed in 3.3. Twelve gates presented correlations higher than moderate positive with ΔNO_2^- and eleven with ΔN_2O (supplementary information S7) with the highest positive correlations for G21_C with ΔNO_2^- (0.8) and with ΔN_2O (0.9).

The correlation of microbiome dynamics to absolute current density and *CE* should also be considered in a BES. The current density presented strong positive correlation to ΔNO_3^- (0.9),

thus only subcommunities previously correlated to ΔNO_3^- presented at least moderate positive correlations to current density (G2 at all sampling ports, G6_B, G9_B). Again, G2 presented the highest correlation to current density (0.5 - 0.7) and also to CE (G2_B 0.6 and G2_C 0.7). Since G2 was the most abundant gate, it suggested that the cells in this subcommunity played a relevant role for the bioelectrochemical nitrate reduction.

Considering all stress-tests (ST-1 to ST-7) for correlation analysis (supplementary information S8), the increase of G2 cell abundance with the increase of ΔNO_3^- and absolute current density (Figure 3, ST-2 to ST-4, ST-6 and ST-7) is also confirmed (correlation values between 0.6 and 0.7 for ΔNO_3^- and 0.6 to 0.8 for current density depending on the SP). A small number of gates showed also at least moderate positive correlation to ΔNO_3^-, ΔNO_2^- or ΔN_2O without a general trend over all sampling ports (supplementary information S8).

Based on the above described dynamics and correlations, it can be concluded that in this d-BES, nitrate was mainly reduced by subcommunity G2, while a wider group of subcommunities were responsible for NO_2^- and N_2O reduction. These cytometric results were supported by conventional functional gene analysis performed on microbial community samples.[17] Denitrifying functional genes napA, narG, nirS and nosZ were successfully amplified, but not nirK. The amplified genes were sequenced, a high diversity was found for every single gene and *Thiobacillus* sp. was identified as contributor to nitrate reduction by narG gene.

Identifying key subcommunity. As a consequence of correlation results, the cells in subcommunity G2 were further investigated on a representative sample (day 95 at SP-C). The molecular analysis showed a predominance of the betaproteobacterium *Thiobacillus* sp. in G2. *Thiobacillus* sp. contributes to the geochemical iron cycling, performing Fe(II)-dependent nitrate-reduction.[32] Electric currents through natural conductive minerals have been demonstrated between *Geobacter sulfurreducens* and *Thiobacillus denitrificans*, suggesting electrotroph capability for *Thiobacillus*.[33] Furthermore, we took samples from the d-BES to inoculate 18 mL-microcosms, which demonstrated that a biofilm predominantly covered by *Thiobacillus* sp. was able to reduce nitrate to nitrite using the electrode as electron donor at a mid-point potential of -0.30V vs. Ag/AgCl.[29] This value was similar to the mid-point potential found for a denitrifying biocathode predominantly covered by betaproteobacteria.[16]

The relevance of *Thiobacillus* sp. was also supported by molecular analyses of microbial community samples taken within the cathode compartment (supplementary information S10). T-RFLP analyses showed an enrichment of *Thiobacillus* sp. from 0% (below the detection limit) in all sampling ports (day 31), to values between 25 and 33% (day 83).

Taking together all results, in the evaluated d-BES, nitrite and nitrous oxide reduction were catalyzed by a number of subcommunities, while nitrate reduction was mainly performed by a single, *Thiobacillus* sp. dominated subcommunity.

Conclusions

Engineering and monitoring are key factors for full-scale applications of denitrifying-BES. In this study, we aimed to use cytometric fingerprinting combined with 16S rDNA analysis and sequencing to monitor a denitrifying biocathode and to derive structure-function relationships of its microbiome.

Different stress-tests were applied simulating events that could occur in full-scale denitrifying-BES. Stress-tests provoked shifts in reactor performance. Among other operational strategies, the stress-tests suggested that the operation at low influent nitrate concentration and low HRT promotes higher denitrification rates.

As a result of the reactor performance variations, dynamics on the biocathodic microbiome were expected, which were fast and effectively monitored using flow cytometry. The monitoring campaign revealed functional relevant subcommunities, which were further confirmed with phylogenetic analysis. A microbial subcommunity mainly composed of *Thiobacillus* sp. was the major contributor to the bioelectrochemical reduction of nitrate to nitrite. While the reduction of NO_2^- and N_2O was performed by a wide number of microbial subcommunities. The further characterization of different bacteria catalyzing each reaction as well as the interplay of these species will contribute to improve nitrate treatment in BES by understanding their specific requirements and behavior under different operational conditions (e.g. cathode potential, or medium composition).

The workflow followed in this study allowed not only investigating the microbiome dynamics, but also enabled to find relevant microbial subcommunities that were catalyzing the individual denitrification steps. Certainly, the strategy and the findings need to be proven to be applicable to a wide variety of reactors and METs. We are confident that the followed strategy can serve as role model for future analysis of BES microbiomes.

Acknowledgements

This work was supported by the Spanish Government (CTQ2011-23632, CTQ2014-SGR-1168) and the Helmholtz-Association within the Research Programme Terrestrial Environment. F.H. acknowledges support by the BMBF (Research Award “Next generation biotechnological processes – Biotechnology 2020+”) and the Helmholtz-Association (Young Investigators Group). N.P. was supported by the Catalan Government (2012FI-B00941) and the University of Girona (MOB2014-ref22).

References

1 B.T. Nolan, B.C. Ruddy, K.J. Hitt and D.R. Helsel, *Environ. Sci. Technol.*, 1997, **31**, 2229–2236, DOI: 10.1021/es960818d.

2 S.P. Seitzinger, R.V. Styles, E.W. Boyer, R.B. Alexander, G. Billen, R.W. Howarth, B. Mayer and N. Van Breemen, *Biogeochemistry*, 2002, **57-58**, 199–237, DOI: 10.1023/A:1015745629794.
3 U. Schröder, F. Harnisch and L.T. Angenent, *Energ. Environ. Sci.*, 2015, **8**, 513-519, DOI: 10.1039/C4EE03359K.
4 Z. He and L.T. Angenent, L.T., *Electroanal.*, 2006, **18**, 2009-2015, DOI: 10.1002/elan.200603628.
5 M. Rosenbaum, F. Aulenta, M. Villano and L.T. Angenent, *Bioresource Technol.*, 2011, **102**, 324-333, DOI: 10.1016/j.biortech.2010.07.008.
6 K.B. Gregory and D.R. Lovley, *Environ. Sci. Technol.*, 2005, **39**, 8943-8947, DOI: 10.1021/es050457e.
7 N. Pous, B. Casentini, S. Rossetti, S. Fazi, S. Puig and F. Aulenta, *J. Hazard. Mater.*, 2015a, **283**, 617-622, DOI: 10.1016/j.jhazmat.2014.10.014.
8 L. Huang, X. Chai, G. Chen and B.E. Logan, *Environ. Sci. Technol.*, 2011, **45**, 5025-5031, DOI: 10.1021/es103875d.
9 K.B. Gregory, D.R. Bond and D.R. Lovley, *Environ. Microbiol.*, 2004, **6**, 596–604, DOI: 10.1111/j.1462-2920.2004.00593.x.
10 P. Clauwaert, K. Rabaey, P. Aelterman, L. De Schamphelaire, T.H. Pham, P. Boeckx, N. Boon and W. Verstraete, *Environ. Sci. Technol.*, 2007, **41**, 3354–3360, DOI: 10.1021/es062580r.
11 Y. Zhang and I. Angelidaki, *Water Res.*, 2013, **47**, 1827–1836, DOI: 10.1016/j.watres.2013.01.005.
12 P. Clauwaert, P. Aelterman, T.H. Pham, L. De Schamphelaire, M. Carballa, K. Rabaey and W. Verstraete, Appl. *Environ. Microb.*, 2008, **79**, 901–913, DOI: 10.1007/s00253-008-1522-2.
13 S. Puig, M. Coma, J. Desloover, N. Boon, J. Colprim and M.D. Balaguer, *Environ. Sci. Technol.*, 2012, **46**, 2309–2315, DOI: 10.1021/es2030609.
14 T. Van Doan, T.K. Lee, S.K. Shukla, J.M. Tiedje and J. Park, *Water Res.*, 2013, **47**, 7087–7097, DOI: 10.1016/j.watres.2013.08.041.
15 B. Virdis, K. Rabaey, Z. Yuan, R.A. Rozendal and J. Keller, *Environ. Sci. Technol.*, 2009, **43**, 5144–5149, DOI: 10.1021/es8036302.
16 K.P. Gregoire, S.M. Glaven, J. Hervey, B. Lin and L.M. Tender, *J. Electrochem. Soc.*, 2014, **161**, H3049-H3057, DOI: 10.1149/2.0101413jes.
17 A. Vilar-Sanz, S. Puig, A. García-Lledó, R. Trias, M.D. Balaguer, J. Colprim and L. Bañeras, *PLoS One*, 2013, **8**, e63460, DOI: 10.1371/journal.pone.0063460.
18 K.C. Wrighton, B. Virdis, P. Clauwaert, S.T. Read, R.A. Daly, N. Boon, Y. Piceno, G.L. Andersen, J.D. Coates and K. Rabaey, *ISME J.*, 2010, **4**, 1443–1455, DOI: 10.1038/ismej.2010.66.
19 F. Harnisch, C. Koch, S. Patil, T. Hübschmann, S. Müller, S. and U. Schröder, *Energ. Environ. Sci.*, 2011, **4**, 1265-1267, DOI: 10.1039/c0ee00605j.
20 F. Harnisch and K. Rabaey, *ChemSusChem*, 2012, **5**, 1012-1019, DOI: 10.1002/cssc.201100732.
21 C. Koch, S. Günther, A.F. Desta, T. Hübschmann and S. Müller, *Nat. Protoc.*, 2013a, **8**, 190–202, DOI: 10.1038/nprot.2012.149.
22 S. Müller and G. Nebe-Von-Caron, *FEMS Microbiol. Rev.*, 2010, **34**, 554–587, DOI: 10.1111/j.1574-6976.2010.00214.x.
23 N. Pous, S. Puig, M. Coma, M.D. Balaguer and J. Colprim, *J. Chem. Technol. Biot.*, 2013, **88**, 1690-1696, DOI: 10.1002/jctb.4020.
24 K. Rabaey, W. Ossieur, M. Verhaege and W. Verstraete, *Water Sci. Technol.*, 2005, **52**, 515–523.
25 N. Pous, S. Puig, M.D. Balaguer and J. Colprim, *Chem. Eng. J.*, 2015b, **263**, 151-159, DOI: 10.1016/j.cej.2014.11.002.
26 Ansys. Ansys fluent theory guide. Inc Northbrook IL**,** 2009, 49–53.
27 C. Koch, I. Fetzer, T. Schmidt, H. Harms and S. Müller, *Environ. Sci. Technol.*, 2013b, **47**, 1753–1760, DOI: 10.1021/es3041048.
28 J. Schumann, C. Koch, S. Günther, I. Fetzer and S. Müller, 2014. FlowCyBar: Analyze flow cytometric data using gate information. R package version 1.2.1.
29 N. Pous, C. Koch, J. Colprim, S. Puig and F. Harnisch, *Electrochem. Commun.*, 2014, **49**, 93-97; DOI: 10.1016/j.elecom.2014.10.011.
30 Y. Xiao, Y. Zheng, S. Wu, Z.H. Yang and F. Zhao, *Microbial Ecol.*, 2014, **69**, 492-499, DOI: 10.1007/s00248-014-0492-4.
31 C. Dancey and J. Reidy, 2004. Statistics without maths for psychology: using SPSS for Windows, London, Prentice Hall.
32 K.L. Straub, M. Benz, B. Schink, and F. Widdel, *Appl. Environ. Microbiol.*, 1996, **62**, 1458–1460.
33 S. Kato, K. Hashimoto and K. Watanabe, P. Natl. Acad. Sci. USA, 2012, **109**, 10042–10046, DOI: 10.1073/pnas.1117592109.